INSTITUTE OF PLASMA PHYSICS

NAGOYA UNIVERSITY

RESEARCH REPORT

NAGOYA, JAPAN

AN ENHANCED SCATTERING OF NEUTRALIZED ELECTRON BEAM ALONG MAGNETIC FIELD

Johshin Uramoto

IPPJ-228 August 1975

Further comminication about this report is to be sent to the Research Information Center, Institute of Plasma Physics, Nagoya University, Nagoya, Japan.

ABSTRACT

When a negative radial electric field is applied externally around an electron beam neutralized critically by passing through a neutral gas in a uniform magnetic field, a radial electron current is produced after a Bohm-likely enhanced mobility. In this state, the electron beam is scattered with an "axially" enhanced collision up to a few per cent of the radial Bohm collision ($\omega_{ce}/16$). That collision may be due to a fluctuating ion space charge left behind by the radial enhanced electron current.

INTRODUCTION

It has been pointed out theoretically by Weinstock[1] that a radial enhanced diffusion across a magnetic field B is accompanied by an anomalous increase in axial electrical resistivity or effective collision frequency along B. Experimentally, it has been reported from microwave conductivity measurements that the effective collision frequency along B becomes as large as 10 times the electron-neutral collision frequency in a turbulent positive column[2] or a diffusional plasma from RF discharge.[3] Their turbulent states across B are induced by a helical instability or a drift dissipative instability while their neutral (He or Ne) pressures drop near 10^{-2} mmHg.

Indirectly, the collective collisions between electron beam and ions has been described theoretically[4] by Buneman, though a radial diffusion and a shielding effect of ion electric fields due to background thermal electrons are not discussed.

Similarly, some plasma heating experiments[5] have been tried by injecting an electron beam along B into a neutral gas. There, a radial electric field and electron current across B are produced automatically through the beam space charge and some instabilities while a high density plasma above the beam density is generated. That is, plasma, electric fields, instabilities and currents are produced almost coincidently. Therefore, relations between their parameters are not clarified analytically.

In this paper, an axially enhanced collision of an electron beam passing through a characteristic plasma in a uniform magnetic field B is investigated in relation with a radially turbulent plasma state. The characteristic plasma density at the center is nearly equal to the electron beam density, which decays radially across B. From another standing point, the electron beam is neutralized by thermal ions critically. The other remarkable point is that a negative radial electric field across B is applied externally to the characteristic plasma while a plus voltage is given to the cylindrical chamber wall for the central electron beam column earthed at the source.

Thus, first, the plasma turbulent state can be controlled by the voltage applied to the chamber wall. Second, the radial enhanced collision frequency through the radial electron mobility can be estimated easily from the radial electron current corresponding to the applied voltage. Third, the axial effective collision frequency can be estimated from a reduction of the electron beam current along B which determines a mean free path (since the beam velocity is known from the accelerating voltage). Finally, a difference between the radial diffusion (ambipolar) and only the radial electron flow (in ions confined radially) can be clarified in relation with the axial enhanced collision.

THEORETICAL CONCEPTIONS

A drift instability is expected by a radial negative

field and electron current across B from the following reasons: Each radial distribution of the electric field $E_\perp$ or the current density $j_\perp$ is initially estimated by $E_\perp(r) = V_o/[r\ell n(R/r_o)] \propto 1/r$ or $j_\perp(r) = I_{\perp o}/(2\pi rL) \propto 1/r$ where V_o, R, r_o, $I_{\perp o}$ and L are the applied voltage, cylindrical chamber radius, primary plasma column radius, radial total current and a plasma length along B. Thus, a radial input power density distribution $j_\perp E_\perp$ is estimated by $j_\perp E_\perp \propto 1/r^2$. On the other hand, when the voltage V_o is not applied, the initial radial distribution of the plasma density n(r) has been estimated from the ordinary diffusion theory[6] by $n(r) \propto \exp(-r/q)$ for $r >> q$ where q is an e-folding length of the plasma radial distribution. Therefore, a radial input power distribution per particle is estimated by $w(r) = j_\perp E_\perp/n(r) \propto \exp(r/q)/r^2$. Here, if $r > 2q$, we find that $\partial w/\partial r > 0$ is satisfied. That is, an input power density per particle is larger outside of the plasma column. From these estimations, for a radial electron temperature (T) gradient, we may assume $\partial T/\partial r > 0$, if the input energy is determined by a particle loss time along B which is independent of radius. Thus, we can expect a drift wave growth condition[7] from $\partial T/\partial r > 0$ and the density gradient $\partial n/\partial r < 0$ (always) by $d\ell n(T)/d\ell n(n) < 0$.

From the drift instability, an enhanced effective collision will generate for the radial direction across B, whose frequency approaches to a corresponding cyclotron angular frequency (Bohm-like collision). Then, the centrifugal forces (mv_θ^2/r) of the azimuthal plasma rotation will

be neglected under a strong collision equilibrium ($v \frac{\partial v}{\partial r}$ << νv) even if the plasma is collisionless classically. Moreover, if the electric field term ($\mu_\perp E_\perp$) becomes sufficiently large compared with the diffusional term ($D_\perp \nabla n/n$), only electrons will move radially while ions are left behind (and while another group of electrons is supplied along B from the electron beam source). In this state, a collisional azimuthal ion current may appear from a difference between the electron azimuthal drift velocity $v_{\theta e}$ and the ion $v_{\theta i}$. Because the electron azimuthal motions are reduced slightly by the radial motions $v_\perp = \mu_\perp E_\perp$ where $\mu_\perp$ is a radial electron mobility, if ion radial motion is neglected near the central electron beam column. That is, we can approximate $v_{\theta e}$ and $v_{\theta i}$ near the center, by

$$v_{\theta e} = \sqrt{v_\theta^2 - v_\perp^2}\ , \quad \cdots\cdots\cdots\cdots (1)$$

$$v_{\theta i} \approx v_\theta = E_\perp / B\ , \quad \cdots\cdots\cdots\cdots (2)$$

where v_θ is an azimuthal drift velocity. From eqs.(1) and (2), the ion azimuthal current density is estimated approximately under $v_\theta >> v_\perp$, by

$$j_{\theta i} = en(v_{\theta i} - v_{\theta e}) \approx en v_\perp \left[\frac{1}{2}\left(\frac{v_\perp}{v_\theta}\right)\right] . \quad \cdots (3)$$

Here, if the radial electron flows after a Bohm-likely enhanced collision frequency ($\omega_{ce}/16$) where ω_{ce} is an electron cyclotron angular frequency, the radial electron

current density $j_{\perp e}$ and the ion azimuthal current $j_{\theta i}$ are determined by, using $v_\perp/v_\theta \approx (\omega_{ce}/16)/\omega_{ce} = 1/16$,

$$\left.\begin{aligned} |j_{\perp e}| &= |en v_\perp| = \left|en\left(\frac{e\nu_B}{m\omega_{ce}^2}\right)E_\perp\right| \\ \nu_B &= \omega_{ce}/16 \end{aligned}\right\}, \quad \cdots\cdots (4)$$

$$\left.\begin{aligned} |j_{\theta i}| &= |en v_\perp[1/32]| = \left|en\left(\frac{e\nu_T}{m\omega_{ce}^2}\right)E_\perp\right| \\ \nu_T &= \nu_B/32 = \omega_{ce}/512 \end{aligned}\right\}, \quad \cdots\cdots (5)$$

where m and e are an electron mass and charge. From these expressions, it is considered that ion space charge fluctuations are produced behind at an "effective" frequency up to 1/32 of the Bohm collision frequency $\omega_{ce}/16$. This background ion charge fluctuations may scatter the electron beam injected along B.

EXPERIMENTAL STUDY

A schematic of the apparatus is shown in Fig.1. A cylindrical electron beam is produced along a uniform magnetic field B = 2 kG, which has an energy of 1 keV and a current of 30 mA in a diameter of 8 mm. A neutralization of the electron beam is adjusted through ionizations of helium gas (He) fed between two anodes A_1 and A_2. The vacuum chamber consists of glass tubes of 10 cm in diameter and a metal mesh tube M is inserted in the measuring region

between the anode A_2 and an end target with a Faraday cup FC of 16 mm in a diameter. The mesh tube M (10 cmϕ) is connected to an external dc power supply in order to produce a radial electric field between the chamber wall and the electron beam column earthed through two anodes. Then, two insulating plates G_1 and G_2 with each central hole are inserted to avoide electrical shorts of the electrode surfaces across B. A length of the measuring region along B is 35 cm. A Langmuir probe is inserted at the middle point of the measuring region, which is movable radially.

A standard neutral pressure between two anodes A_1 and A_2 is determined as $P = 3.0 \times 10^{-3}$ mmHg (beam energy loss due to ionizations < 1 eV) under a neutralized condition that the ionized ion density n_i in the measuring region ($P \lesssim 2 \times 10^{-4}$ mm Hg) is nearly equal to the beam electron density n_b. The ion density is measured from the thermal plasma density by the Langmuir probe characteristic on the beam column surface, which corresponds to about $n_b \approx n_i \approx 2.0 \times 10^8$/cc for the electron beam current I_o = 30 mA (the energy 1 keV and the cross-section 0.5 cm^2). The thermal electron (produced by the beam) temperature is about 16 eV near the beam column, and the thermal electron current to the end Faraday cup is negligible compared with the beam electron current since $v_{th}/v_b < 10^{-1}$ where v_{th} and v_b are the thermal electron velocity and the beam electron velocity. Moreover, the thermal electron current component is cut by a negative bias voltage ($\approx$ -50 V) applied to the Faraday cup. (The neutralization time[8] due to the electron beam is

estimated about 0.5 μsec at $P = 3.0 \times 10^{-3}$ mmHg).

When a voltage V_o is applied to the chamber wall mesh M, the ion density inside of the beam decreases abruptly if the voltage polarity is minus. However, as shown in Fig.2, if the polarity is plus, the ion density is kept above 1/2 of the initial density even if the voltage increases up to the beam accelerating voltage 1 kV. Then, the ion density fluctuation increases up to $\delta n/n = 1.0$ with the plus applied voltage, whose frequency increases (towards the ion cyclotron frequency ω_{ci} = 760 kHz) also as shown in Fig.3. An azimuthal mode in the ion fluctuation is observed at $m_\theta = 1$, which shows the azimuthal drift due to the negative radial electric field and the axial magnetic field B.

The electron beam currents $I(z_o)$ to the end Faraday cup are determined as shown in Fig.4 while the mesh applied voltage V_o is varied at plus or minus sign. The electron beam current under the minus sign is reduced critically near the beam accelerating voltage after the ions are lost almost as understood from Fig.2. On the other hand, the electron beam current under the plus sign decreases monotonously with the voltage while a radial electron current $\Delta I_\perp$ flows below 1/10 of a reduction $\Delta I_\parallel$ in the axial electron beam current. Radial wall potential distributions are shown in Fig.5 (also, shown in Fig.17 of Appendix) while the applied voltage is varied. It should be noted that the wall potentials drop near the beam column nevertheless the applied potentials V_o are plus, and that the dropped regions of the wall potential are spread radially

with the plus applied voltages.

DISCUSSION

We can consider that the critical reduction of the electron beam current under the minus applied voltage is due to only an electro-static repelling potential. However, in the case where the plus voltage is applied, the reduction of the neutralized electron beam current is not explained from the electro-static potential effect. Moreover, the classical electron-ion or neutral collision mean free path ($\lambda_{ei} \gtrsim 10^9$ cm or $\lambda_{en} \gtrsim 10^4$ cm) is much longer than the axial measuring region 35 cm.

Usually, the axial effective mean free path λ for the electron beam may be determined classically

$$I(z_o) = I_o \exp(-z_o/\lambda), \quad \cdots\cdots\cdots (6)$$

where I_o and $I(z_o)$ are an initially injected current (= $I(z_o)$ at $V_o = 0$) and a reduced current (for $V_o \neq 0$) at the end $z_o = L = 35$ cm. Then, the axial collision frequency $\nu_{\parallel ef}$ is given by

$$\nu_{\parallel ef} = v_b/\lambda, \quad \cdots\cdots\cdots (7)$$

where v_b is the electron beam velocity determined from the accelerating voltage. From eqs. (6) and (7), we obtain

$$\nu_{\parallel ef} = v_b \cdot \ln\{I_o / I(z_o)\} \cdot / z_o \quad \cdots\cdots (8)$$

Using the present experimental conditions z_o = 35 cm, $[I_o/I(z_o)]_{max} \approx 2.0$ (as seen in Fig.4) at the applied voltage V_o = 900 V and the electron beam velocity $v_b = 1.87 \times 10^9$ cm/sec at V_b = 1 keV, we obtain $\nu_{\parallel ef} \approx 3.7 \times 10^7$/sec. This, axial collision frequency much exceeds above the electron-ion collision frequency $\nu_{ei} \lesssim 1$ Hz and electron-neutral collision frequency $\nu_{en} \lesssim 10^5$ Hz.

On the other hand, the radial effective collision $\nu_{\perp ef}$ through the electron radial mobility $\mu_\perp$ can be estimated from the radial electron current $\Delta I_\perp$ if the radial electric field is large sufficiently. The radial electron current is estimated by $\Delta I_\perp = en(r_o)v_\perp S_\perp(r_o)$ where $n(r_o)$ and $S_\perp(r_o)$ is an electron density and a surface area along B at the beam column radius $r = r_o$. Here, it is known experimentally as shown in Fig.6 or (in Fig.16 of Appendix) that the radial plasma density gradient outside of the beam column, decreases below 1/R when the applied voltage increases (where R is a chamber tube radius). Therefore, if the radial electric field $E_\perp >> V_e/R$ where V_e is the electron temperature (exactly, a radial component of the electron beam), the radial electron velocity $v_\perp$ is determined by the electric field $E_\perp$ and the radial electron mobility $\mu_\perp$ since the radial electron pressure gradient term (diffusion term) is neglected. That is, $v_\perp \approx \mu_\perp E_\perp$. Experimentally, the approximation is allowed for $|E_\perp| >> 3$ V/cm since $V_e \approx 16$ eV

and $R \gtrsim 5$ cm. Thus, experimentally, above the applied voltage $V_o \gtrsim 200$ V, the radial electron current $\Delta I_\perp$ is expressed by

$$\Delta I_\perp = e\, n(r_o)\, \mu_\perp E_\perp S_\perp(r_o), \quad \cdots\cdots (9)$$

$$\mu_\perp = \Delta I_\perp / \{ e\, n(r_o) E_\perp S_\perp(r_o) \}, \quad \cdots\cdots (9)'$$

where $S_\perp(r_o)$ is given by $2\pi r_o L$ (L is the measuring region length along B). Using the experimental conditions ($\Delta I_\perp \gtrsim 10^{-3}$ A, $n(r_o) \gtrsim 10^8$/ccm $E_\perp \gtrsim -50$ V/cm and $S_\perp(r_o) \gtrsim 8 \times 10^2$ cm^2) at $V_o \simeq 900$ V, we obtain $\mu_\perp \gtrsim 1.5 \times 10^3$ cm^2/V·sec. On the other hand, if a Einstein relation is alowed, the radial Bohm like enhanced mobility μ_B is theoretically estimated by

$$\mu_B = D_B / V_e = \frac{1}{16} \frac{10^8}{B}, \quad \cdots\cdots\cdots (10)$$

where D_B means the Bohm diffusion coefficient. For the present magnetic field B = 2 kG, we obtain $\mu_B \gtrsim 3 \times 10^3$ cm^2/V·sec. Thus, it is found that the experimental mobility $\mu_\perp$ is near the Bohm like mobility μ_B. Similarly, the radial effective collision frequency is estimated to be $\nu_{\perp ef} \gtrsim 10^9$/sec from $\nu_{\perp ef} = \frac{e}{m\mu_\perp}$. The ratio between the axial and radial effective collision $\nu_{\parallel ef}/\nu_{\perp ef}$ is about 0.04 at V_o = 900 V. Thus, we can find that an influence of the radial enhanced collision appears also in the axial direction at 4%. The radially spread potential drop as seen in Fig.5 means a large scattering of beam electrons by the enhanced

collision $\nu_{\parallel ef}$ along B.

Usually, a deflection time of a charged test particle is nearly equal to a slowing down time. This slowing down effect along B is observed as a reflection of the electron beam current. The current reflection is determined from the current increments to the two anodes (A_1, A_2) currents while the beam current to the end Faraday cup is reduced by the applied voltage V_o. For V_o < 1000 V, about 80 % of the reduced current $\Delta I_\parallel$ is reflected as the anode sides currents.

Here, two relations between the radial current and the reduced current $\Delta I_\parallel = I_o - I(Z_o)$ are estimated by a current ratio $\alpha = \Delta I_\perp / \Delta I_\parallel$ and a power ratio $\beta = (\Delta I_\perp \cdot V_o)/(\Delta I_\parallel \cdot V_b)$, where V_o and V_b are the applied voltage and the beam accelerating voltage. For V_o < 1000 V, we observe that $\alpha \gtrsim 1/12$ and $\beta \lesssim 1/12$. From a current conservation, it is considered that $\Delta I_\perp \gtrsim (1 - \gamma)\Delta I_\parallel$ where γ is a reflection rate of $\Delta I_\parallel$ ($\gtrsim 0.8$ at the present experiment). That is, $\Delta I_\perp / \Delta I_\parallel \gtrsim (1 - \gamma)$. Thus, the current ratio α shows an absorption rate of $\Delta I_\parallel$.

Roughly, α is estimated by, from the current conservation,

$$\alpha = \Delta I_\perp / \Delta I_\parallel \approx \frac{e \Delta n v_\perp S_\perp(r_o)}{e \Delta n v_b S_\parallel(r_o)}$$

$$\simeq v_\perp 2L/(v_b r_o), \quad \cdots\cdots\cdots\cdots (11)$$

where r_o and Δn are the electron beam radius and the elec-

tron density at r_o, and $S_\perp(r_o) = 2\pi L r_o$ and $S_\parallel(r_o) = \pi r_o^2$. Using the experimental conditions $v_\perp \gtrsim 10^5 \sim 10^6$ cm/sec, $v_b \gtrsim 2 \times 10^9$ cm/sec and $2L/r_o \gtrsim 2 \times 10^2$, we can estimate to be $\alpha = 1/10^2 \sim 1/10$. However, for $V_o > 1000$ V, the current ratio α increases abruptly above 1.0 while the beam current reduction $\Delta I_\parallel$ saturates. Moreover, the current reflections to the two anodes cease. That means that $\Delta I_\perp$ increases independently of $\Delta I_\parallel$ for $V_o > 1000$ V. This state is connected with a radial discharge due to a residual neutral gas, which is easily judged from the plasma density increment and the plasma wall potential rising. Thus, it is found that the applied voltage shows a collisional "grid action" for the neutralized electron beam before a radial discharge. Obviously, a restriction for $I_{min}(Z_o) \equiv (I_o - \Delta I_\parallel)_{min}$ is given by $I_{min}(Z_o) >> \Delta I_\parallel$. Therefore, when $I(Z_o)$ decreases near $\Delta I_\perp$, the grid action is not allowed. It should be noted that the applied voltage sign is plus, and that a large part of ions are confined.

A dependence of the axial collision frequency $\nu_{\parallel ef}$ on the magnetic field B is understood from Figs.7 and 8. Using eq.(8), we can estimate that $\nu_{\parallel ef}$ is proportional to B and near a few per cent of $\omega_{ce}/16$. Next, a dependence of $\nu_{\parallel ef}$ on the electron beam energy is understood from Figs.9 and 10. As a result, the axial effective collision frequency is nearly independent of the beam energy V_b, because $[v_b \cdot \ell n\{I_o/I_{min}(Z_o)\}]$ is nearly constant since $v_b \propto \sqrt{V_b}$. Similarly, a dependence of $\nu_{\parallel ef}$ on the axial measuring region length (Z_o) is investigated. Then, we find, as

shown in Fig.11 that $Z_o \ell n\{I_o/I_{min}(Z_o)\}$ is nearly constant if V_b = const. Thus, the effective collision frequency $\nu_{\parallel ef}$ is independent of Z_o also.

Experimentally, we find that the electron temperature increases radially as shown in Fig.12, when V_o is applied. Therefore, it is considered that the instability which produces the radial Bohm-likely enhanced mobility, is due to a drift wave growth[7] from a radial positive temperature gradient $\partial T/\partial r > 0$ (since the radial density gradient is negative as demonstrated in Figs.6 or 16).

From this radial positive temperature gradient and the ratio for the radial Bohm collision $\omega_{ce}/16$, we may consider a mechanism as described in "Theoretical Conceptions".

Finally, within $\alpha = \Delta I_\perp/\Delta I_\parallel \lesssim 1/10$, a ratio $I_o/I_{min}(Z_o)$ between the initially injected current and a minimum current at the end is investigated varying production methods of neutralized electron beam as shown in Appendix. Then, we find under B = 1.0 kG as shown in the Appendix that the current ratio $I_o/I_{min}(Z_o)$ is about 3.3 at $\bar{V}_b \approx 300$ V and I_o = 0.6 A ($n_b \approx 10^{10}$/cc). In this case, the neutralized electron beam is produced from an electron beam like discharge. As a result, we cna estimate a mean free path and an effective collision frequency from eq.(8). That is, $\lambda \approx 29$ cm and $\nu_{\parallel ef} = 3.3 \times 10^7$/sec at $\bar{V}_b \approx 300$ V, while the Bohm like collision frequency $\omega_{ce}/16$ and the experimental values $\nu_{\perp ef}$ is about 10^9/sec. Thus, we find also, independently of the current density and the neutralized electron beam production methods, that the effective colli-

sion frequency increases up to a few per cent of the Bohm-like collision within $\alpha = 1/10 \sim 1/30$ and $\beta = 1/10 \sim 1/20$. This result should be compared with the Buneman instability where the effective collision frequency depends on the electron beam density at $(m/M)^{1/3}\omega_{pe}$.

However, if the electron beam density n_b decreases abruptly as shown in Fig.13. This result may indicate that interactions between ions and electrons are reduced at a low density. (The Debye length at $n = 10^7$/cc and $V_e = 15$ eV is comparable with the electron beam diameter.)

The radial electric field $E_\perp$ must be sufficiently large compared with the pressure gradient term V_e/q (V_e: electron temperature in eV, q: radial density e-folding length). This condition is related with the mesh tube radius R where the external voltage is applied. For $R > 4$ cm, $E_\perp >> V_e/q$ is satisfied experimentally. However, for $R < 2.5$ cm, the electric field condition is not satisfied, because the radial electric field drops abruptly while the thermal electron current flows to the mesh tube, and α increases above 1/4. They mean that the applied voltage V_o does not operate for the beam as a powerless "grid action". For this small mesh tube, the applied voltage V_o operates almost axially and some instabilities or large density fluctuations are not observed ($\delta n/n < 0.2$). Results for the small radius tube may be compared with the electrostatic confinement[9] which is based on repelling forces due to a plus potential for ions and a minus for electrons.

The criterion $E_\perp >> V_e/q$ means that the radial plasma

diffusion must not be ambipolar and that, for $E_\perp < 0$, ions are left behind or driven for the center. Thus, this mechanism which gives an axially enhanced collision to the neutralized electron beam, is different from the Weinstock's theory. His theory will be applied only to a radially and axially diffusional plasma and a plasma in which an electron stream is produced by the axial electric field E_z, that is, a positive column. Obviously, in our experiments, the axial electric field E_z is not present initially. Therefore, the helical or screw type instability is not considered. Similarly, since the electron-ion or neutral collision is negligible classically, the drift dissipative instatility is not considered also.

The oscillation in the ion density is not always turbulent, but nearly monochromatic. In typical experiments[10] and theories[11] on enhanced diffusion under a strong turbulence, a monochromatic ion oscillation below ω_{ci} has been observed and predicted. The characteristic oscillation is determined by a balance[11] between a maximum ion wave growth factor and a damping factor due to the ion enhanced transport. In our experiment, as shown in Fig.3, an ion oscillation below ω_{ci} is observed also, which produces an ion-electron effective collisoin frequency $(\nu_{ie})_{\perp ef}$. On the other hand, the corresponding electron-ion collision frequency is connected by $(\nu_{ei})_{\perp ef} = (\frac{v_e}{v_i})^2 (\nu_{ie})_{\perp ef}$, where v_e and v_i are an electron and ion thermal velocity. The $(\nu_{ei})_{\perp ef}$ is estimated from the radial electron mobility $\mu_\perp$ through the radial electron current as defined in eq.(9').

For the present experimental conditions, $(\nu_{ei})_{\perp ef} \gtrsim 10^9$/sec and $(\nu_{ie})_{\perp ef} \gtrsim 10^5$/sec are reasonable since $(v_e/v_i) \gtrsim 10^2$.

In conclusion, when a radial electron current flows under a large negative electric field ($E_\perp >> V_e/q$) produced externally, a neutralized electron beam along B is much scattered with an axially enhanced collision which approaches up to a few percent of the radial Bohm-like collision.

REFERENCES

1. J. Weinstock, Phys. Rev. Lett. 20, 1149 (1968)
2. T. Tsukishima, A. Mase and S. Takeda, Phys. Fluids 13, 649 (1970)
3. M. Kando and S. Takeda, Kaku Yugo Kenkyu (in Japanese) 29, 358 (1973)
4. O. Buneman, Phys. Rev. 115, 503 (1959)
5. I. Alexeff et al., Phys. Rev. Lett. 25, 848 (1970)
6. F. Boeshoten, Plasma Phys. (J. Nucl. Energy Part C) 6, 339 (1964)
7. B. B. Kadomtsev, Plasma Turbulence (Academic Press, London, New York, 1965) Chap.IV
8. E. G. Linder and K. G. Hernqvist, J. Appl. Phys. 21, 1088 (1950)
9. R. W. Moir, W. L. Barr and P. F. Post, Phys. Fluids 14, 2531 (1971)
10. N. S. Buchel'nikova et al., Zh. Eksp. Teor. Fiz. 52, 837 (1967); Sov. Phys. JETP 25, 548 (1967)
11. T. H. Dupree, Phys. Fluids 10, 1049 (1967)

FIGURE CAPTIONS

Fig.1. Schematic diagram of apparatus. A_1, A_2: anodes. K: cathode. G_1, G_2: insulating plates. M: metal mesh tube (10 cmϕ). FC: end Faraday cup. P: probe. V_o: applied voltage. V_B: negative bias voltage (-20 $\sim$ -50 V). V_b: beam accelerating voltage (1 kV). $\vec{B}$: uniform amgnetic field (2 kG).

Fig.2. Dependences of normalized ion density (n/n_o) on applied voltages V_o. $\oplus$: plus V_o. $\ominus$: minus V_o.

Fig.3. Dependence of ion density fluctuation amplitude ($\delta n/n$) and frequency (f) on applied voltage (plus) V_o.

Fig.4. Dependence of axial beam current $I(Z_o)$ to end Faraday cup on applied voltage V_o or radial current $\Delta I_\perp$ (plus V_o). I_o: initial beam current (at $V_o = 0$). $\oplus$: plus V_o. $\ominus$: minus V_o.

Fig.5. Radial distributions of plasma wall potential V_W for various applied voltages. r: radius at middle point. (1): $V_o = 0$. (2): $V_o = 450$ V. (3): $V_o = 750$ V. (4): $V_o = 1000$ V. (5): $V_o = -300$ V.

Fig.6. Dependence of normalized radial plasma density distribution (n/n_o) on applied voltage V_o. $I(Z_o)$ = 30 ∿ 18 mA. B = 2.0 kG. r: radius.. (1): V_o = 0. (2): V_o = 250 V. (3): V_o = 500 V. (4): V_o = 750 V (from ion saturation current to Langmuir probe with -400 V bias). V_b = 1 kV.

Fig.7. Dependence of axial beam current $I(Z_o)$ on magnetic field B. I_o: initial beam current (at V_o = 0). V_o: applied voltage. V_b: beam accelerating voltage. B_1: 0.6 kG (I_o = 18 mA). B_2: 1.2 kG (I_o = 22 mA). B_3: 1.8 kG (I_o = 29 mA).

Fig.8. Dependence of axial current parameter ξ on magnetic field B (corresponding to Fig.7). $\xi \equiv \ell n\{I_o/I_{min}(Z_o)\}$. $\nu''_{ef} = 5.4 \times 10^7\ \xi$/sec.

Fig.9. Dependence of axial current $I(Z_o)$ on beam accelerating voltage V_b at B = 1.0 kG. (1): V_b = 250 V (I_o = 4.4 mA). (2): V_b = 500 V (I_o = 9.7 mA). (3): V_b = 1 kV (I_o = 23.0 mA). (4): V_b = 1.5 kV (I_o = 38.0 mA).

Fig.10. Dependence of axial current parameter ξ on beam accelerating voltage V_b (corresponding to Fig.9). $\xi \equiv \ell n\{I_o/I_{min}(Z_o)\}$. $\nu''_{ef} = 5.4 \times 10^7 \xi\sqrt{V_b}$/sec ($V_b$; kV).

Fig.11. Dependence of axial current parameter ξ on axial measuring region length (Z_o). V_b = 1 kV. B = 2.0 kG. $\xi \equiv \ell n\{I_o/I_{min}(Z_o)\}$. I_o = 30 mA.

Fig.12. Radial electron temperature distributions at applied voltage $V_o = 0$ and $V_o \neq 0$. (1): $V_o = 0$. (2): $V_o \approx 350$ V. B = 1.0 kG. V_b = 1 kV. $I(Z_o)$ = 24 ∿ 18 mA.

Fig.13. Dependence of axial current parameter ξ on beam current I_o. $\xi \equiv \ell n\{I_o/I_{min}(Z_o)\}$. $\nu''_{ef} = 5.7 \times 10^7$ ξ/sec. V_b = 1.1 kV. B = 1.5 kG. n_b: beam electron density.

Fig.14. Experimental apparatus of Appendix. S_1, S_2: slit electrodes (-300 V, 6 A). Cathode region pressure: 1.2×10^{-2} mmHg in He. Measuring region pressure: 3.5×10^{-4} mmHg in He.

Fig.15. Dependence of axial current $I(Z_o)$ to end Faraday cup on applied voltage V_o or radial current $\Delta I_\perp$ (Appendix). I_o: initial beam current. Magnetic field B = 1.0 kG.

Fig.16. Dependence of relative radial plasma density distribution (n/n_o) on applied voltage V_o (Appendix). r: radisu. (1): $V_o = 0$. (2): V_o = 100 V. (3): V_o = 200 V. (4): V_o = 400 V. B = 1.0 kG. I_o = 0.6 A. $\bar{V}_b \approx 300$ V.

Fig.17. Radial plasma wall potential distribution V_W for various applied voltage V_o (Appendix). (1): V_o = 0. (2): V_o = 200 V. (3): V_o = 400 V. B = 1.0 kG. $\bar{V}_b \approx$ 300 V. I_o = 0.6 A.

APPENDIX

A schematic of the neutralized electron beam source is shown in Fig.14. First, a dc discharge is fired between an oxide cathode K and two slit electrodes S_1 and S_2, where the gas (He) pressure is about 1.2×10^{-2} mmHg and the discharge current is about 6 A (at 40 V). Next, a high electron beam is produced between an anode A and a slit S_1 where the helium pressure is 3.5×10^{-4} mmHg and an accelerating voltage (300 V) is kept automatically. The magnetic field is uniform at B = 1.0 kG. Thus, a neutralized electron beam with an energy 300 eV and a current 0.6 A (0.8 cmϕ) is injected into the measuring region ($\sim 3.0 \times 10^{-4}$ mmHg in He) as shown in Fig.14.

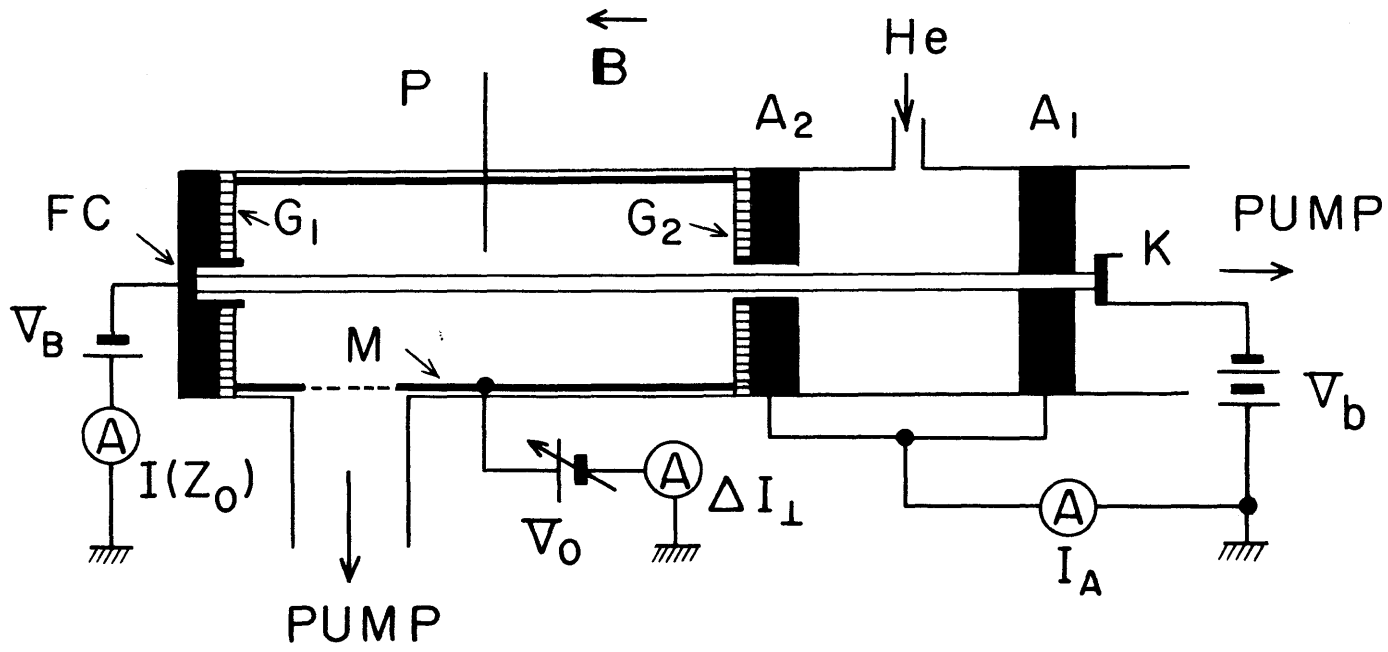

Fig. 1

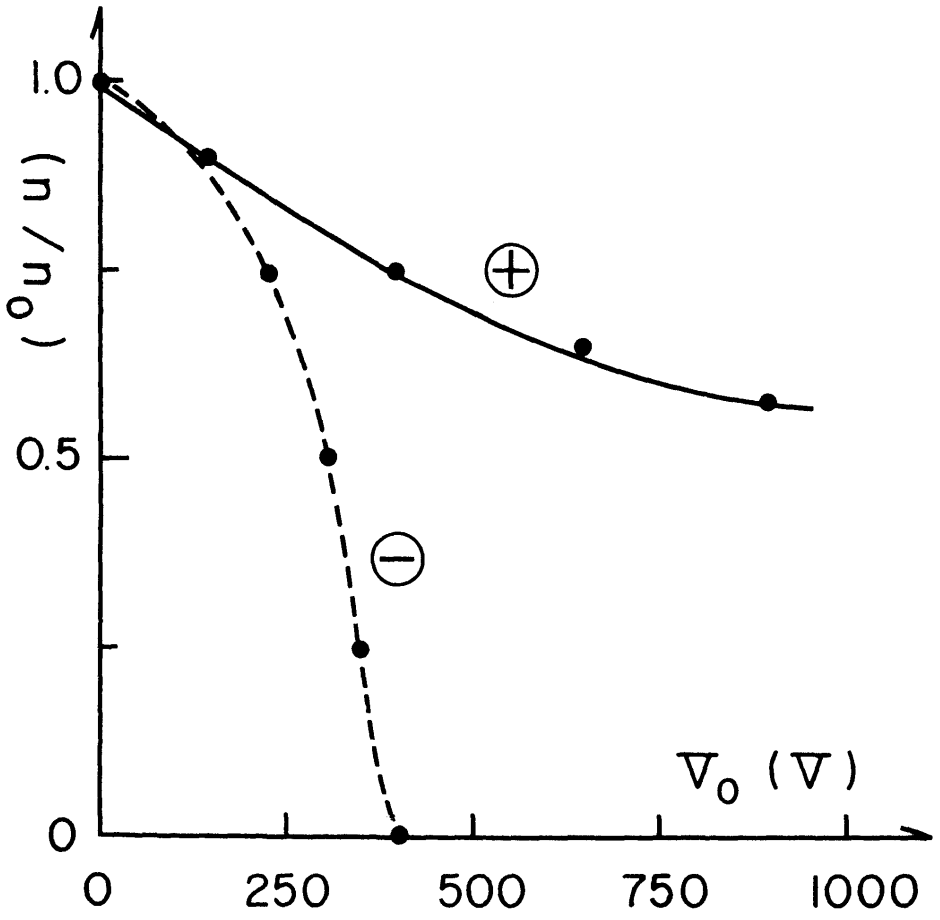

Fig. 2

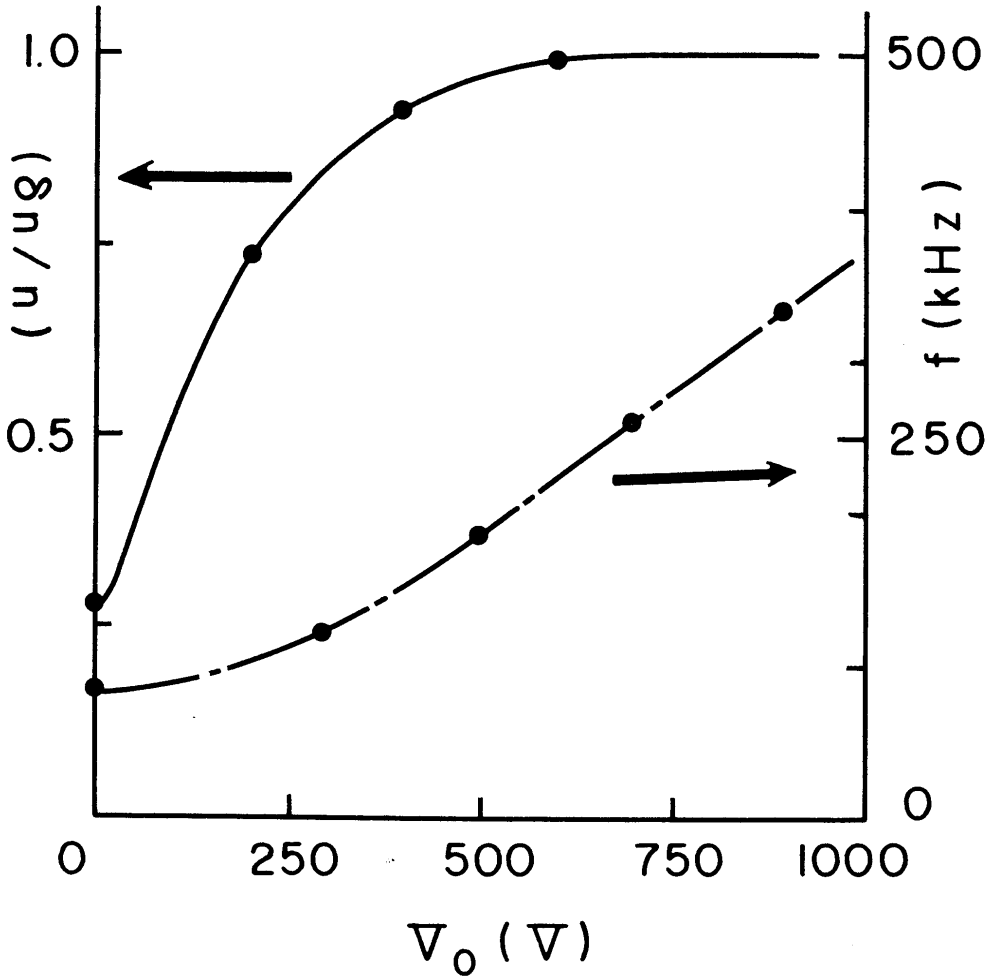

Fig. 3

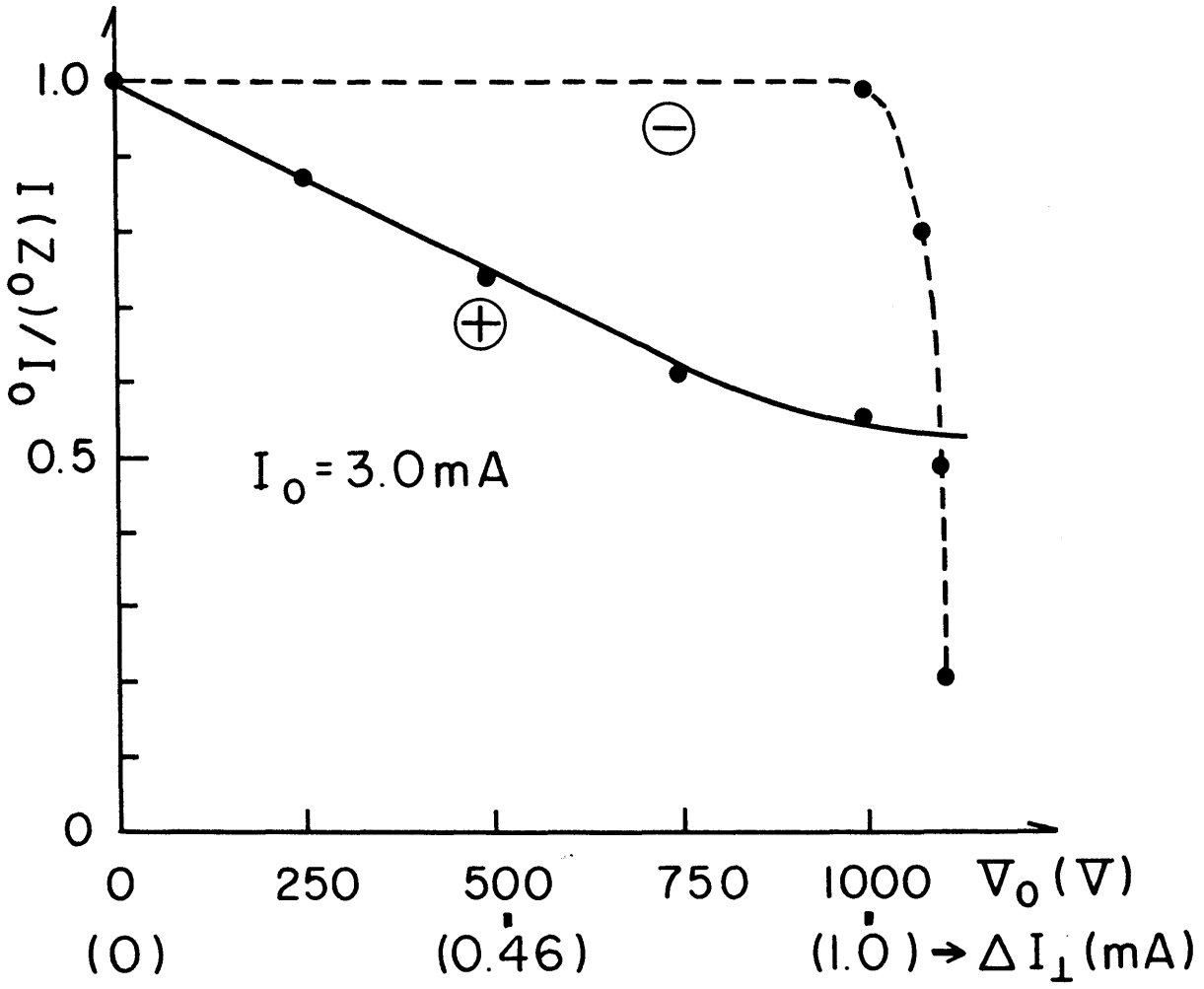
1.0
0.5
0
$^{o}I/(^{o}Z)I$
⊖
⊕
$I_o = 3.0mA$
0
250
500
750
1000
$V_o(V)$
(0)
(0.46)
(1.0) → $\Delta I_\perp$ (mA)

Fig. 4

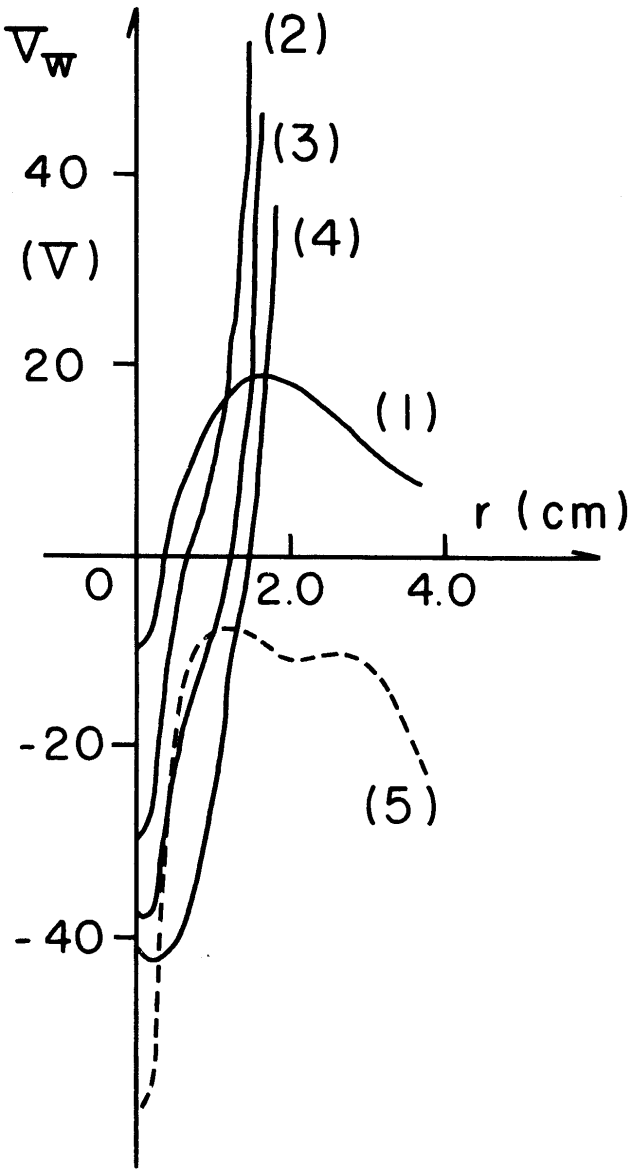

Fig. 5

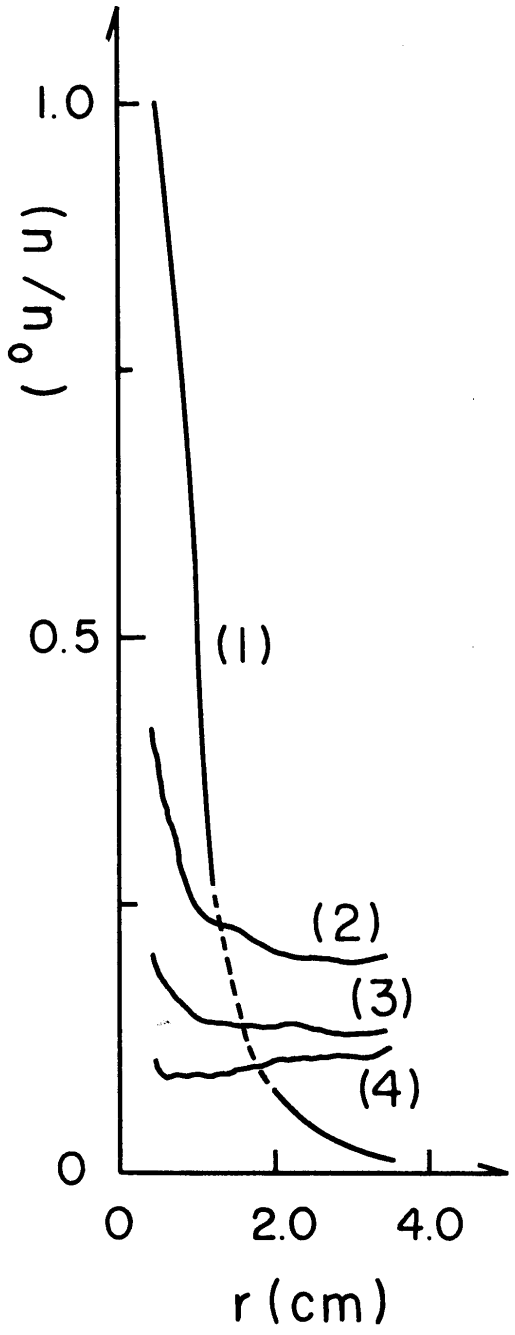

Fig. 6

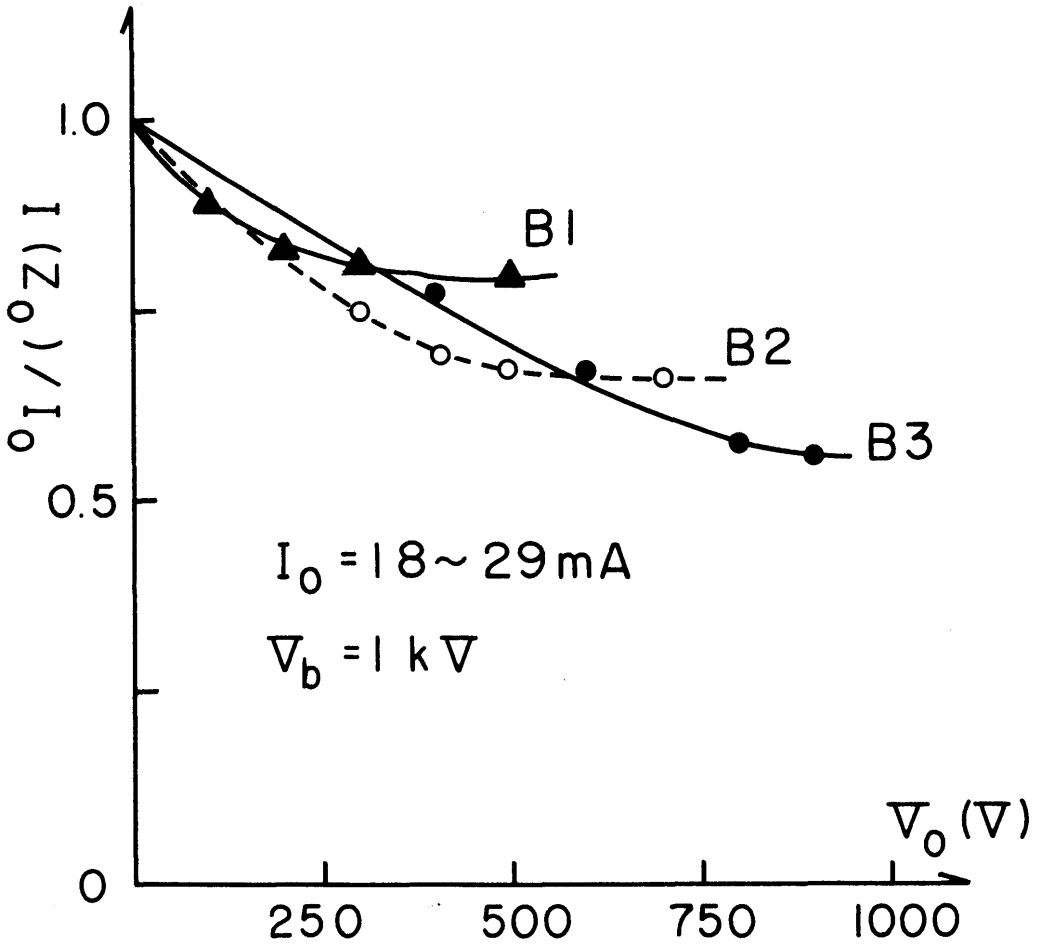

Fig. 7

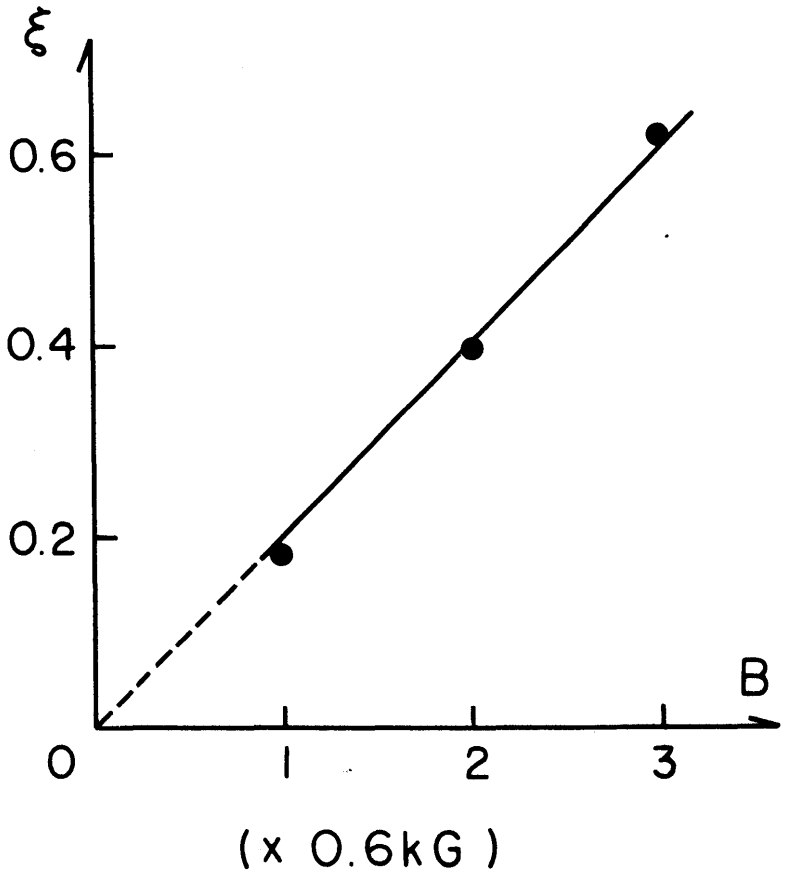

Fig.8

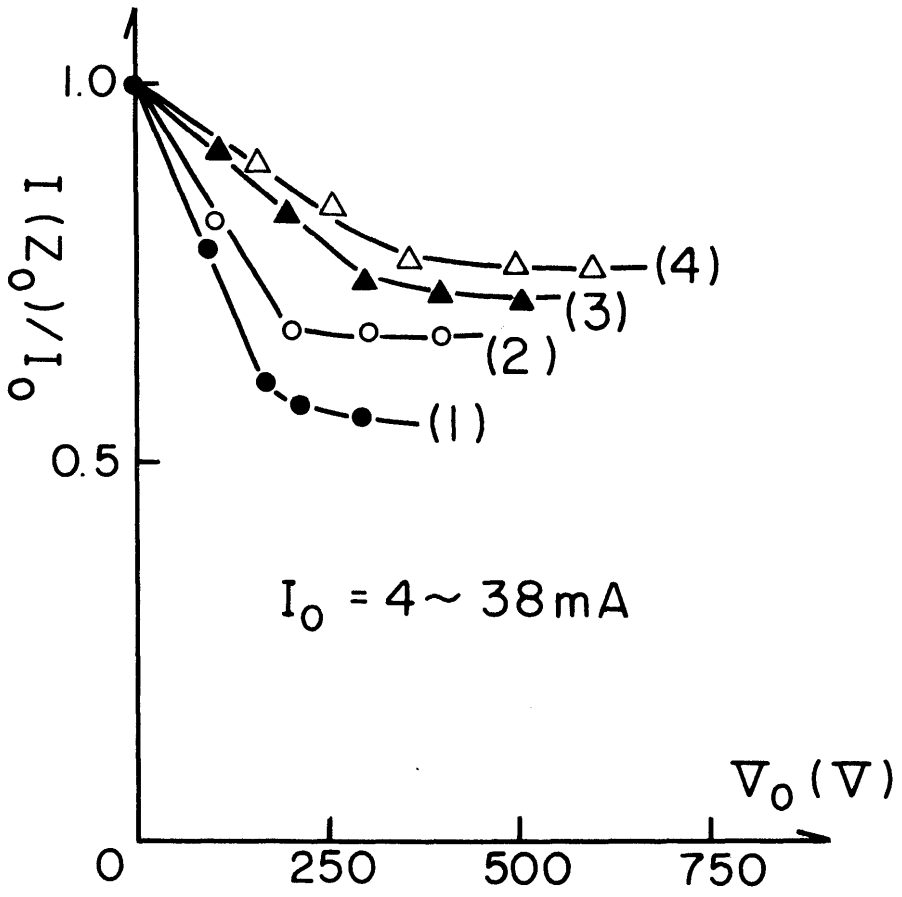

Fig. 9

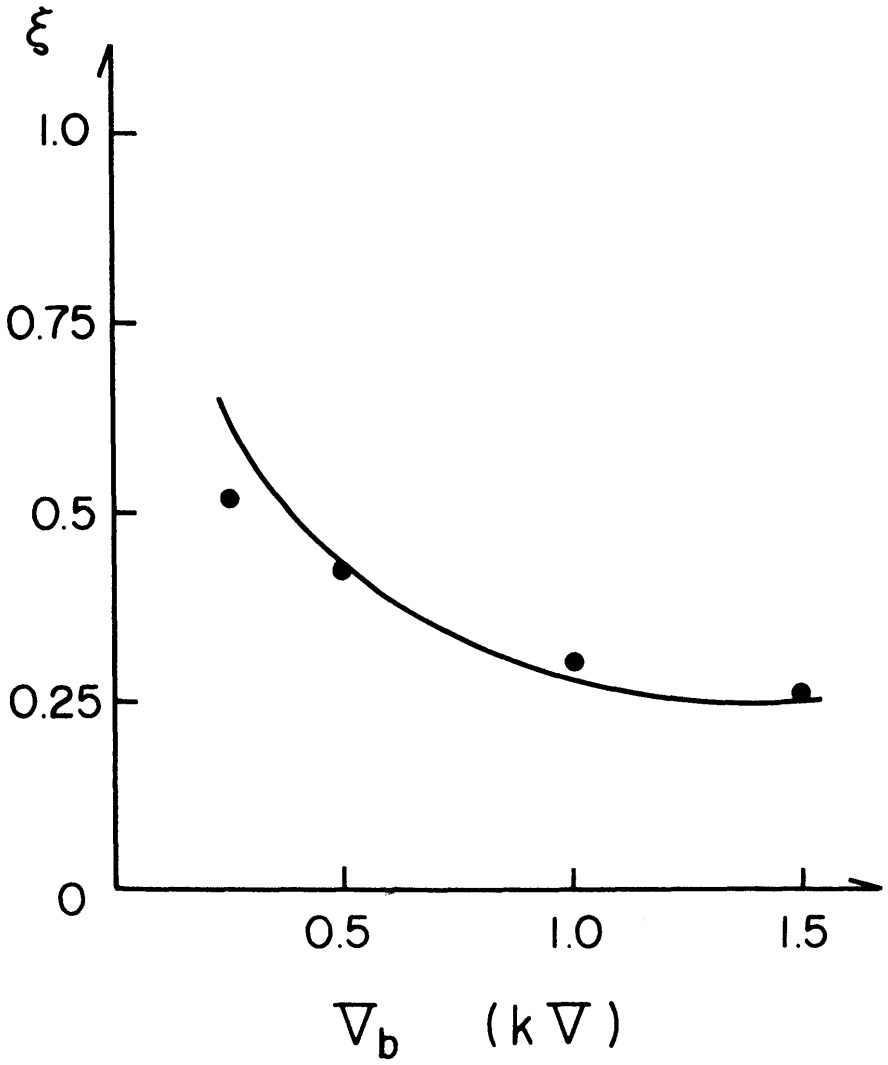

Fig. 10

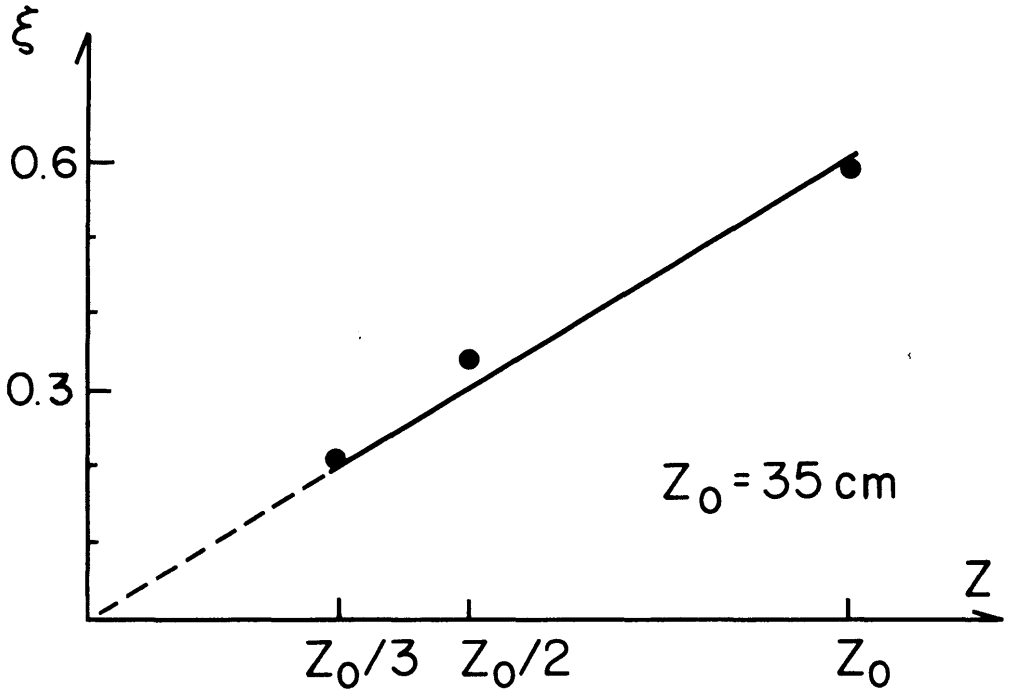

Fig. 11

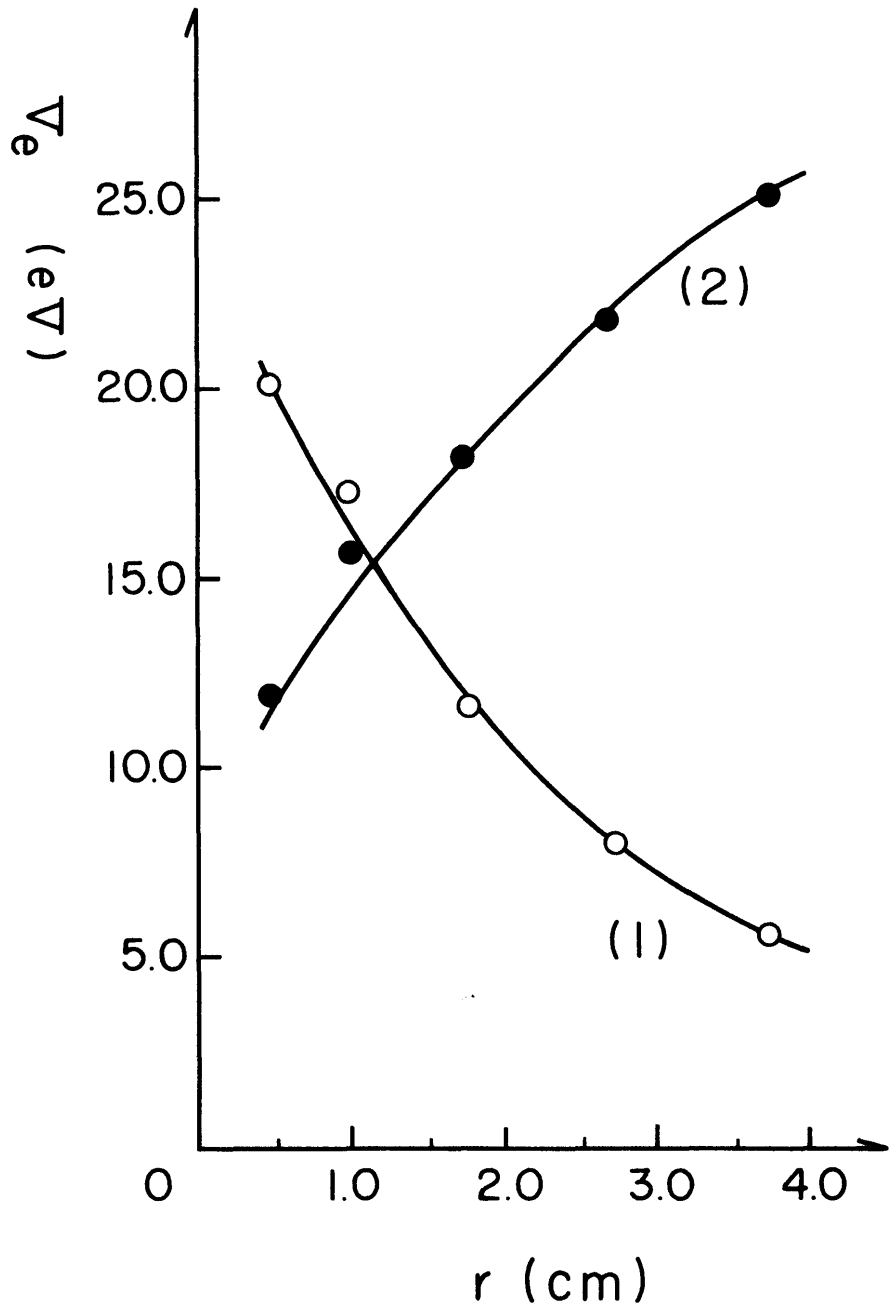

Fig. 12

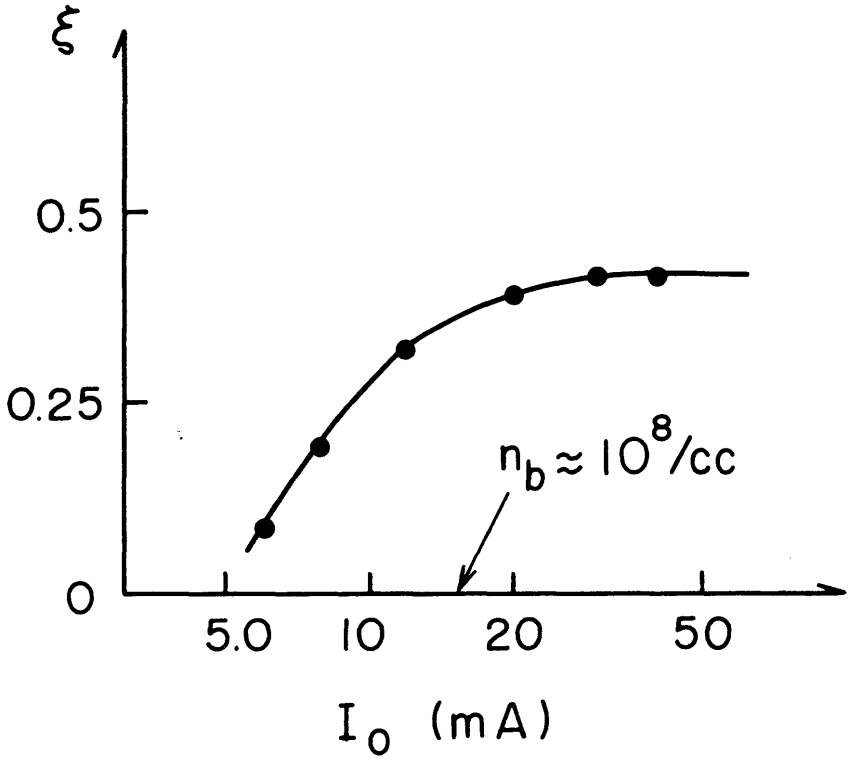

Fig. 13

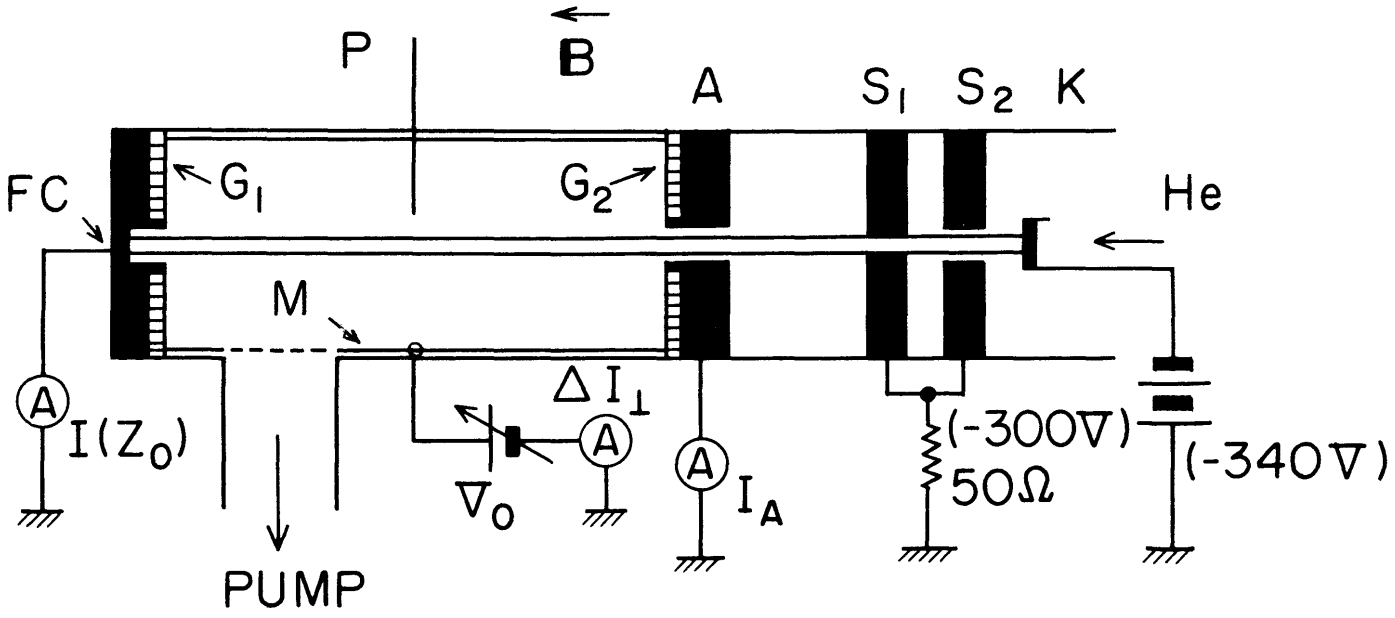

Fig. 14

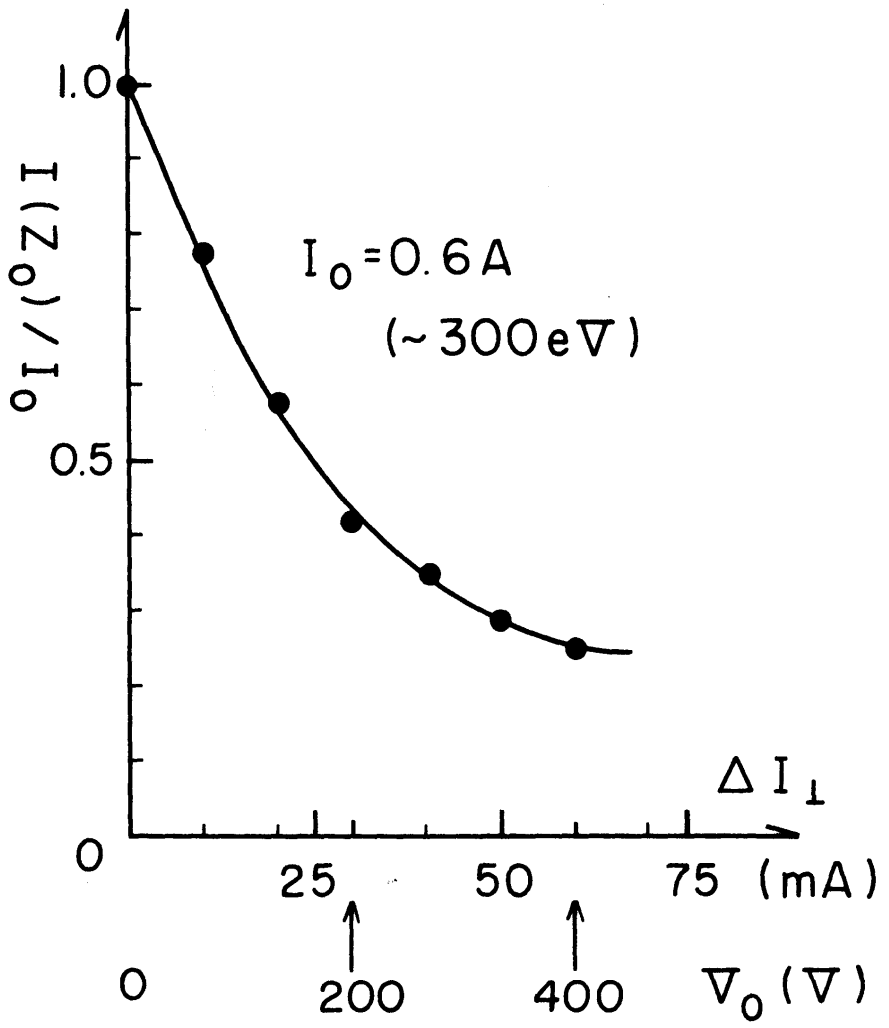
1.0
0.5
0
$I(Z_0)/I_0$
$I_0 = 0.6A$
$(\sim 300 eV)$
$\Delta I_\perp$
25
50
75 (mA)
0
200
400
V_0 (V)

Fig. 15

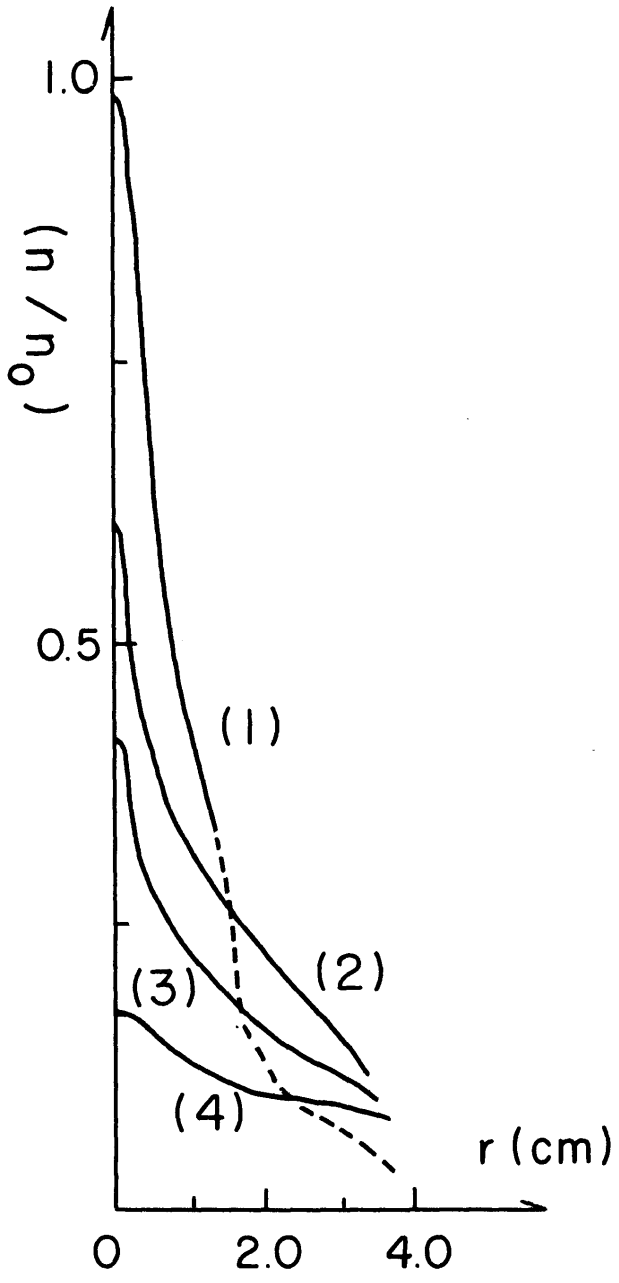

Fig. 16

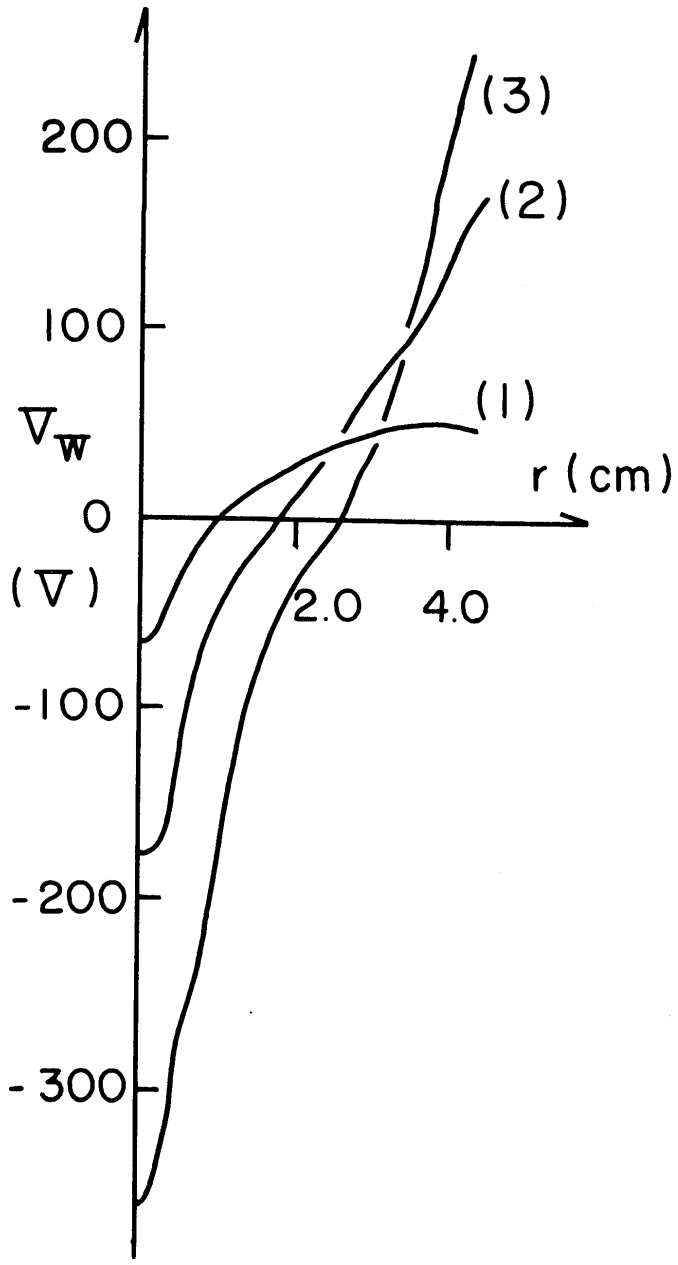

Fig. 17